Northumbria Research Link

Citation: Vo, Thuc and Lee, Jaehong (2010) Geometrically nonlinear analysis of thin-walled open-section composite beams. Computers & Structures, 88 (5-6). 347 - 356. ISSN 0045-7949

Published by: Elsevier

URL: http://dx.doi.org/10.1016/j.compstruc.2009.11.007 <http://dx.doi.org/10.1016/j.compstruc.2009.11.007>

This version was downloaded from Northumbria Research Link: http://nrl.northumbria.ac.uk/id/eprint/13382/

Northumbria University has developed Northumbria Research Link (NRL) to enable users to access the University's research output. Copyright © and moral rights for items on NRL are retained by the individual author(s) and/or other copyright owners. Single copies of full items can be reproduced, displayed or performed, and given to third parties in any format or medium for personal research or study, educational, or not-for-profit purposes without prior permission or charge, provided the authors, title and full bibliographic details are given, as well as a hyperlink and/or URL to the original metadata page. The content must not be changed in any way. Full items must not be sold commercially in any format or medium without formal permission of the copyright holder. The full policy is available online: http://nrl.northumbria.ac.uk/policies.html

This document may differ from the final, published version of the research and has been made available online in accordance with publisher policies. To read and/or cite from the published version of the research, please visit the publisher's website (a subscription may be required.)

Northumbria University NEWCASTLE

University Library

*Revised Manuscript (without changes highlighted)

Geometrically nonlinear analysis of thin-walled open-section composite beams

Thuc Phuong Vo* and Jaehong Lee†

Department of Architectural Engineering, Sejong University
98 Kunja Dong, Kwangjin Ku, Seoul 143-747, Korea

(Dated: August 26, 2009)

A geometrically nonlinear model for general thin-walled open-section composite beams with arbitrary lay-ups under various types of loadings based on the classical lamination theory is presented. It accounts for all structural coupling coming from the material anisotropy and geometric nonlinearity. Nonlinear governing equations are derived and solved by means of an incremental Newton-Raphson method. The finite element model that accounts for the geometric nonlinearity in the von Karman sense is developed to solve the problem. Numerical results are obtained for thin-walled composite Z-beam and I-beam to investigate effects of geometric nonlinearity, fiber orientation and warping restraint on the flexural-torsional response.

Keywords: Thin-walled composite beams; classical lamination theory; flexural-torsional response; nonlinear theory

I. INTRODUCTION

Fiber-reinforced composite materials have been used over the past few decades in a variety of structures. Composites have many desirable characteristics, such as high ratio of stiffness and strength to weight, corrosion resistance and magnetic transparency. Thin-walled composite structures are often very thin and have complicated material anisotropy. A large number of practical problems of thin-walled composite structures require a geometrically nonlinear formulation, such as the post-buckling behavior, load carrying capacity of structures used in aeronautical, aerospace as well as in mechanical and civil engineering. However, their structural behavior is very complex due to coupling effects as well as warping-torsion and therefore, the accurate prediction of geometrically nonlinear response is one of the fundamental importance in the design of composite structures.

*Graduate student

†Professor, corresponding author. Tel.:+82-2-3408-3287; fax:+82-2-3408-3331

; Electronic address: jhlee@sejong.ac.kr

The theory of thin-walled open-section members made of isotropic materials was first developed by Vlasov [1] and Gjelsvik [2]. In the development of a geometrically nonlinear beam element, basically an updated Lagrangian or a total Lagrangian formulation can be employed. These formulations must be implemented using appropriate displacement interpolation functions. Bathe and Bolourchi [3] presented two consistent large rotation nonlinear three dimensional beam formulations: an updated Lagrangian and a total Lagrangian formulation for a 2-node Hermitian interpolation beam. Although a large number of studies have been performed on the geometrically nonlinear analysis of isotropic thin-walled structures, it should be noted that only a few deal with nonlinear flexural-torsional behavior of thin-walled composite beams with arbitrary lay-ups. A literature survey on the subject shows that there appears some works reported on geometrically nonlinear theory for thin-walled composite beams. The studies of this theory for these members carried out so far may broadly be divided into two groups. The first and most common approach is based on an analytical technique, while the other approach requires a two-dimensional finite element analysis to obtain the cross-section stiffness matrix. Atilgan and Hodges et al. [4-9] pioneered the second approach, which was referred to as the so-called "Variational Asymptotic Beam Section Analysis". Hodges and co-workers (e.g., Cesnik et al. [5], Volovoi et al.[6], Yu et al. [7-9] further applied the concept introduced by variational asymptotic method to two dimensional cross-sectional problem and derived closed-form expressions for the cross-sectional stiffness coefficients of thin-walled beams. In the present investigation, an analytical approach is adopted for the derivation of the cross-sectional stiffness matrix considering different effects and their coupling to yield a general formulation. Bauld and Tzeng [10] presented nonlinear model for thin-walled composite beams by extending Gjelsvik's formulation to the balanced symmetric laminated composite materials. However, the formulation was somewhat not consistent in the sense that it used coordinate mapping when developing nonlinear stresses instead of variational formulation. Gupta and Rao [11,12] developed finite element analysis to study instability of thin-walled open-section laminated composite beams. The nonlinear expressions for the strains occurring in thin-walled open-section beams under axial, flexural and torsional loads, were incorporated in a general instability analysis. Bhaskar and Librescu [13,14] developed non-linear theory of thin-walled composite beams, which were employed in a broad field of engineering problems. In these models, the transverse shear deformation was taken into account but the warping torsion component was neglected. By extending model of Bauld and Tzeng [10], Omidvar and Ghorbanpoor [15] derived a nonlinear finite element analysis for thin-walled open-section composite beams with symmetric stacking sequence based on the updated Lagrangian formulation. Fraternali and Feo [16] formulated a small strain and moderate rotation theory of laminated composite thin-walled beams by generalizing the classical Vlasov theory. This beam model accounted for axial, bending, torsion

and warping deformations and allowed one to predict critical loads and initial post-buckling behavior. Rajasekaran and Nalinaa [17] presented a detailed treatment of the formulation of static, bucking and vibration analysis of non-prismatic thin-walled composite spatial members of generic section. The theory was limited to small strains, moderate deflections and small rotations. Special attention deserved the works of Machado, Cortinez and Piovan [18,19,20] who introduced a geometrically non-linear theory for thin-walled composite beams for both open and closed cross-sections and taking into account shear flexibility (bending and warping shear). This non-linear formulation was developed by using a non-linear displacement field, whose rotations were based on the rule of semi-tangential transformation. It was used for analyzing the stability of thin-walled composite beam with general cross-section. However, it was strictly valid for symmetric balanced laminates and especially orthotropic laminates. Cardoso et al. [21] developed a finite element model for structural analysis of composite laminated thin-walled beam structures, with geometrically nonlinear behavior, including post-critical behavior and warping deformation.

In this paper, the analytical model developed by the authors [22] is extended to the geometric nonlinearity. Based on the variational formulation, a geometrically nonlinear model for general thin-walled open-section composite beams with arbitrary lay-ups under various types of loads is given. This model is based on the classical lamination theory, and accounts for all the axial-flexural-torsional coupling coming from the material anisotropy and geometric nonlinearity. The nonlinear governing equations are derived and solved by means of an incremental Newton-Raphson method. A displacement-based one-dimensional finite element model that accounts for the geometric nonlinearity in the von Kármán sense is developed to solve the problem. Numerical results are obtained for thin-walled composite Z-beam and I-beam under vertical load to investigate the effects of fiber orientation, warping restraint and load parameter on the nonlinear flexural-torsional response.

II. KINEMATICS

The theoretical developments presented in this paper require two sets of coordinate systems which are mutually interrelated. The first coordinate system is the orthogonal Cartesian coordinate system (x, y, z), for which the x and y axes lie in the plane of the cross section and the z axis parallel to the longitudinal axis of the beam. The second coordinate system is the local plate coordinate (n, s, z) as shown in Fig.1, wherein the n axis is normal to the middle surface of a plate element, the s axis is tangent to the middle surface and is directed along the contour line of the cross section. The (n, s, z) and (x, y, z) coordinate systems are related through an angle of orientation θ. As defined in Fig.1 a point P, called the pole, is placed at an arbitrary point x_p, y_p. A line through P parallel to the z axis is

called the pole axis.

To derive the analytical model for a thin-walled composite beam, the following assumptions are made:

1. The contour of the thin wall does not deform in its own plane.

2. The linear shear strain $\bar{\gamma}_{sz}$ of the middle surface is zero in each element.

3. The Kirchhoff-Love assumption in classical plate theory remains valid for laminated composite thin-walled beams.

According to assumption 1, the midsurface displacement components $\bar{u}, \bar{v}$ at a point A in the contour coordinate system can be expressed in terms of a displacements U, V of the pole P in the x, y directions, respectively, and the rotation angle Φ about the pole axis,

$$\bar{u}(s,z) = U(z)\sin\theta(s) - V(z)\cos\theta(s) - \Phi(z)q(s) \tag{1a}$$

$$\bar{v}(s,z) = U(z)\cos\theta(s) + V(z)\sin\theta(s) + \Phi(z)r(s) \tag{1b}$$

These equations apply to the whole contour. The out-of-plane shell displacement $\bar{w}$ can now be found from the assumption 2. For each element of middle surface, the shear strain become

$$\bar{\gamma}_{sz} = \frac{\partial \bar{v}}{\partial z} + \frac{\partial \bar{w}}{\partial s} = 0 \tag{2}$$

After substituting for $\bar{v}$ from Eq.(1) and considering the following geometric relations,

$$dx = ds\cos\theta \tag{3a}$$

$$dy = ds\sin\theta \tag{3b}$$

Eq.(2) can be integrated with respect to s from the origin to an arbitrary point on the contour,

$$\bar{w}(s,z) = W(z) - U'(z)x(s) - V'(z)y(s) - \Phi'(z)\omega(s) \tag{4}$$

where differentiation with respect to the axial coordinate z is denoted by primes ($'$); W represents the average axial displacement of the beam in the z direction; x and y are the coordinates of the contour in the (x, y, z) coordinate system; and ω is the so-called sectorial coordinate or warping function given by

$$\omega(s) = \int_{s_\circ}^{s} r(s)ds \tag{5a}$$

The displacement components u, v, w representing the deformation of any generic point on the profile section are given with respect to the midsurface displacements $\bar{u}, \bar{v}, \bar{w}$ by the assumption 3.

$$u(s,z,n) = \bar{u}(s,z) \tag{6a}$$

$$v(s,z,n) = \bar{v}(s,z) - n\frac{\partial \bar{u}(s,z)}{\partial s} \tag{6b}$$

$$w(s,z,n) = \bar{w}(s,z) - n\frac{\partial \bar{u}(s,z)}{\partial z} \tag{6c}$$

The von Kármán type strains, in which only the products of u, v and their derivatives are retained and all other nonlinear terms are neglected, are considered and given by

$$\epsilon_z = \frac{\partial w}{\partial z} + \frac{1}{2}\Big[\big(\frac{\partial u}{\partial z}\big)^2 + \big(\frac{\partial v}{\partial z}\big)^2\Big] \tag{7a}$$

$$\gamma_{sz} = \frac{\partial v}{\partial z} + \frac{\partial w}{\partial s} \tag{7b}$$

Eq.(7) can be rewritten as

$$\epsilon_z = \bar{\epsilon}_z + n\bar{\kappa}_z + n^2\bar{\chi}_z \tag{8a}$$

$$\gamma_{sz} = \bar{\gamma}_{sz} + n\bar{\kappa}_{sz} \tag{8b}$$

where

$$\bar{\epsilon}_z = \frac{\partial \bar{w}}{\partial z} + \frac{1}{2}\Big[\big(\frac{\partial \bar{u}}{\partial z}\big)^2 + \big(\frac{\partial \bar{v}}{\partial z}\big)^2\Big] \tag{9a}$$

$$\bar{\kappa}_z = -\frac{\partial^2 \bar{u}}{\partial z^2} - \frac{\partial^2 \bar{u}}{\partial s \partial z}\frac{\partial \bar{v}}{\partial z} \tag{9b}$$

$$\bar{\kappa}_{sz} = -2\frac{\partial^2 \bar{u}}{\partial s \partial z} \tag{9c}$$

$$\bar{\chi}_z = \Big(\frac{\partial^2 \bar{u}}{\partial s \partial z}\Big)^2 \tag{9d}$$

In Eq.(9), $\bar{\epsilon}_z$, $\bar{\kappa}_z, \bar{\kappa}_{sz}$ and $\bar{\chi}_z$ are midsurface axial strain, biaxial curvature and high order curvature of the shell, respectively. The above shell strains can be converted to beam strain components by substituting Eqs.(1), (4) and (6) into Eq.(9) as

$$\bar{\epsilon}_z = \epsilon_z^\circ + x\kappa_y + y\kappa_x + \omega\kappa_\omega \tag{10a}$$

$$\bar{\kappa}_z = \kappa_y \sin\theta - \kappa_x \cos\theta - \kappa_\omega q + \chi_z r \tag{10b}$$

$$\bar{\kappa}_{sz} = \kappa_{sz} \tag{10c}$$

$$\bar{\chi}_z = \chi_z \tag{10d}$$

where $\epsilon_z^\circ, \kappa_x, \kappa_y, \kappa_\omega, \kappa_{sz}$ and χ_z are axial strain, biaxial curvatures in the x and y direction, warping curvature with respect to the shear center, twisting and high order curvature in the beam, respectively defined as

$$\epsilon_z^\circ = W' + \frac{1}{2}\left[U'^2 + V'^2 + (r^2+q^2)\Phi'^2\right] - x_p V'\Phi' + y_p U'\Phi' \tag{11a}$$

$$\kappa_x = -V'' - U'\Phi' \tag{11b}$$

$$\kappa_y = -U'' + V'\Phi' \tag{11c}$$

$$\kappa_\omega = -\Phi'' \tag{11d}$$

$$\kappa_{sz} = 2\Phi' \tag{11e}$$

$$\chi_z = \frac{1}{2}\Phi'^2 \tag{11f}$$

The resulting strains can be obtained from Eqs.(8) and (10) as

$$\epsilon_z = \epsilon_z^\circ + (x + n\sin\theta)\kappa_y + (y - n\cos\theta)\kappa_x + (\omega - nq)\kappa_\omega + (2rn + n^2)\chi_z \tag{12a}$$

$$\gamma_{sz} = n\kappa_{sz} \tag{12b}$$

III. VARIATIONAL FORMULATION

Total potential energy of the system is calculated by sum of strain energy and work done by external forces

$$\Pi = \mathcal{U} + \mathcal{V} \tag{13}$$

where $\mathcal{U}$ is the strain energy

$$\mathcal{U} = \frac{1}{2}\int_v (\sigma_z \epsilon_z + \sigma_{sz}\gamma_{sz})dv \tag{14}$$

The variation of strain energy is calculated by substituting Eq.(12) into Eq.(14)

$$\begin{aligned}\delta\mathcal{U} &= \int_v \left\{\sigma_z\left[\delta\epsilon_z^\circ + (x+n\sin\theta)\delta\kappa_y + (y-n\cos\theta)\delta\kappa_x + (\omega - nq)\delta\kappa_\omega + (2rn+n^2)\delta\chi_z\right] + \sigma_{sz}n\delta\kappa_{sz}\right\}dv \\ &= \int_0^l (N_z\delta\epsilon_z^\circ + M_y\delta\kappa_y + M_x\delta\kappa_x + M_\omega\delta\kappa_\omega + M_t\delta\kappa_{sz} + R_z\delta\chi_z)dz \end{aligned} \tag{15}$$

where $N_z, M_x, M_y, M_\omega, M_t, R_z$ are axial force, bending moments in the x and y directions, warping moment (bi-moment), torsional moment and high order stress resultant with respect to the centroid respectively, defined by

integrating over the cross-sectional area A as

$$N_z = \int_A \sigma_z ds dn \tag{16a}$$

$$M_y = \int_A \sigma_z (x + n\sin\theta) ds dn \tag{16b}$$

$$M_x = \int_A \sigma_z (y - n\cos\theta) ds dn \tag{16c}$$

$$M_\omega = \int_A \sigma_z (\omega - nq) ds dn \tag{16d}$$

$$M_t = \int_A \sigma_{sz} n ds dn \tag{16e}$$

$$R_z = \int_A \sigma_z (2rn + n^2) ds dn \tag{16f}$$

The variation of the strain energy can be obtained by substituting Eqs.(11) and (12) into Eq.(15)

$$\begin{aligned}\delta\mathcal{U} = \int_0^l \Big[& N_z \delta W' - M_y \delta U'' - M_x \delta V'' - M_\omega \delta\Phi'' + 2M_t \delta\Phi' + N_z(U'\delta U' + V'\delta V') \\ + \; & (M_y - x_p N_z)(V'\delta\Phi' + \Phi'\delta V') - (M_x - y_p N_z)(U'\delta\Phi' + \Phi'\delta U') + (r_p^2 N_z + R_z)\Phi'\delta\Phi' \Big] dz \end{aligned} \tag{17}$$

On the other hand, the variation of work done by external forces can be written as

$$\delta\mathcal{V} = -\int_v (p_z \delta w + p_n \delta u + p_s \delta v) dv \tag{18}$$

where p_z, p_n, p_s are forces acting in z, n and s direction. The above expression can be written with respect to the shell forces and displacements by using Eq.(6)

$$\delta\mathcal{V} = -\int_0^l \int_s (\bar{p}_z \delta\bar{w} + \bar{p}_n \delta\bar{n} + \bar{p}_s \delta\bar{v} - \bar{m}_z \frac{\partial\delta\bar{u}}{\partial z} - \bar{m}_s \frac{\partial\delta\bar{u}}{\partial s}) ds dz \tag{19}$$

where $\bar{p}_z, \bar{p}_s, \bar{m}_z, \bar{m}_s, \bar{p}_n$ are shell forces defined by

$$(\bar{p}_z, \bar{m}_z) = \int_n p_z(1, n) dn \tag{20a}$$

$$(\bar{p}_s, \bar{m}_s) = \int_n p_s(1, n) dn \tag{20b}$$

$$\bar{p}_n = \int_n p_n dn \tag{20c}$$

After substituting Eqs.(1) and (4) into Eq.(19), the variation of the work done by the external forces can be written with respect to the bar forces

$$\delta\mathcal{V} = -\int_0^l [\mathcal{P}_z \delta W + \mathcal{V}_x \delta U + \mathcal{M}_y \delta U' + \mathcal{V}_y \delta V + \mathcal{M}_x \delta V' + \mathcal{T}\delta\Phi + \mathcal{M}_\omega \delta\Phi'] dz \tag{21}$$

where the bar forces are related to the shell forces as

$$\mathcal{P}_z = \int_s \bar{p}_z ds \tag{22a}$$

$$\mathcal{V}_y = \int_s (\bar{p}_s \sin\theta - \bar{p}_n \cos\theta) ds \tag{22b}$$

$$\mathcal{V}_x = \int_s (\bar{p}_s \cos\theta + \bar{p}_n \sin\theta) ds \tag{22c}$$

$$\mathcal{T} = \int_s (\bar{p}_s r - \bar{p}_n q + \bar{m}_s) ds \tag{22d}$$

$$\mathcal{M}_y = \int_s (\bar{m}_z \sin\theta - \bar{p}_z x) ds \tag{22e}$$

$$\mathcal{M}_x = \int_s (\bar{m}_z \cos\theta - \bar{p}_z y) ds \tag{22f}$$

$$\mathcal{M}_\omega = \int_s (\bar{m}_z q - \bar{p}_z \omega) ds \tag{22g}$$

Using the principle that the variation of the total potential energy is zero, the weak form of the present theory for thin-walled composite beams are obtained

$$\begin{aligned} 0 = & \int_0^l \Big[N_z \delta W' - M_y \delta U'' - M_x \delta V'' - M_\omega \delta\Phi'' + 2M_t \delta\Phi' + N_z(U'\delta U' + V'\delta V') \\ & + (M_y - x_p N_z)(V'\delta\Phi' + \Phi'\delta V') - (M_x - y_p N_z)(U'\delta\Phi' + \Phi'\delta U') + (r_p^2 N_z + R_z)\Phi'\delta\Phi' \\ & - \mathcal{P}_z \delta W - \mathcal{V}_x \delta U - \mathcal{M}_y \delta U' - \mathcal{V}_y \delta V - \mathcal{M}_x \delta V' - \mathcal{T}\delta\Phi - \mathcal{M}_\omega \delta\Phi' \Big] dz \end{aligned} \tag{23}$$

IV. CONSTITUTIVE EQUATIONS

The constitutive equations of a k^{th} orthotropic lamina in the laminate co-ordinate system are given by

$$\begin{Bmatrix} \sigma_z \\ \sigma_{sz} \end{Bmatrix}^k = \begin{bmatrix} \bar{Q}^*_{11} & \bar{Q}^*_{16} \\ \bar{Q}^*_{16} & \bar{Q}^*_{66} \end{bmatrix}^k \begin{Bmatrix} \epsilon_z \\ \gamma_{sz} \end{Bmatrix} \tag{24}$$

where $\bar{Q}^*_{ij}$ are transformed reduced stiffnesses. The transformed reduced stiffnesses can be calculated from the transformed stiffnesses based on the plane stress ($\sigma_s = 0$) and plane strain ($\epsilon_s = 0$) assumption. More detailed explanation can be found in Ref.[23].

The constitutive equations for bar forces and bar strains are obtained by using Eqs.(12), (16) and (24)

$$\begin{Bmatrix} N_z \\ M_y \\ M_x \\ M_\omega \\ M_t \\ R_z \end{Bmatrix} = \begin{bmatrix} E_{11} & E_{12} & E_{13} & E_{14} & E_{15} & E_{16} \\ & E_{22} & E_{23} & E_{24} & E_{25} & E_{26} \\ & & E_{33} & E_{34} & E_{35} & E_{36} \\ & & & E_{44} & E_{45} & E_{46} \\ & & & & E_{55} & E_{56} \\ \text{sym.} & & & & & E_{66} \end{bmatrix} \begin{Bmatrix} \epsilon_z^\circ \\ \kappa_y \\ \kappa_x \\ \kappa_\omega \\ \kappa_{sz} \\ \chi_z \end{Bmatrix} \tag{25}$$

where E_{ij} are laminate stiffnesses of thin-walled composite beams, and can be defined by

$$E_{16} = \int_s (2B_{11}r + D_{11})ds \tag{26a}$$

$$E_{26} = \int_s \Big[2B_{11}rx + D_{11}(x + 2r\sin\theta) + F_{11}\sin\theta\Big]ds \tag{26b}$$

$$E_{36} = \int_s \Big[2B_{11}ry + D_{11}(y - 2r\cos\theta) - F_{11}\cos\theta\Big]ds \tag{26c}$$

$$E_{46} = \int_s \Big[2B_{11}r\omega + D_{11}(\omega - 2rq) - F_{11}q\Big]ds \tag{26d}$$

$$E_{56} = \int_s (2D_{16}r - F_{16})ds \tag{26e}$$

$$E_{66} = \int_s (4D_{11}r^2 + 4rF_{11} + H_{11})ds \tag{26f}$$

where A_{ij}, B_{ij}, D_{ij} matrices are extensional, coupling, bending stiffness and F_{ij}, H_{ij} matrices are higher order stiffnesses, respectively, defined by

$$(A_{ij}, B_{ij}, D_{ij}, F_{ij}, H_{ij}) = \int \bar{Q}_{ij}(1, n, n^2, n^3, n^4)dn \tag{27}$$

Other values of E_{ij} can be found in Ref.[22]. The explicit forms of the laminate stiffnesses E_{ij} for general I-section are given in the Appendix.

V. GOVERNING EQUATIONS

The nonlinear equilibrium equations of the present study can be obtained by integrating the derivatives of the varied quantities by parts and collecting the coefficients of $\delta W, \delta U, \delta V$ and $\delta\Phi$

$$N_z' + \mathcal{P}_z = 0 \tag{28a}$$

$$M_y'' + [N_z(U' + y_p\Phi')]' - [M_x\Phi']' + \mathcal{V}_x - \mathcal{M}_y' = 0 \tag{28b}$$

$$M_x'' + [N_z(V' - x_p\Phi')]' + [M_y\Phi']' + \mathcal{V}_y - \mathcal{M}_x' = 0 \tag{28c}$$

$$M_\omega'' + 2M_t' + [N_z(r_p^2\Phi' + y_pU' - x_pV')]' + [M_yV']' - [M_xU']' + [R_z\Phi']' + \mathcal{T} - \mathcal{M}_\omega' = 0 \tag{28d}$$

The natural boundary conditions are of the form

$$\delta W \ : \ N_z \tag{29a}$$

$$\delta U \ : \ M_y' + N_z(U' + y_p\Phi') - M_x\Phi' \tag{29b}$$

$$\delta U' \ : \ M_y \tag{29c}$$

$$\delta V \ : \ M_x' + N_z(V' - x_p\Phi') + M_y\Phi' \tag{29d}$$

$$\delta V' \ : \ M_x \tag{29e}$$

$$\delta\Phi \ : \ M_\omega' + 2M_t + N_z(r_p^2\Phi' + y_pU' - x_pV') + M_yV' - M_xU' + R_z\Phi' \tag{29f}$$

$$\delta\Phi' \ : \ M_\omega \tag{29g}$$

Eq.(29g) denotes the warping restraint boundary condition. When the warping of the cross section is restrained, $\Phi' = 0$ and when the warping is not restrained (free warping), $M_\omega = 0$.

By substituting Eqs.(11) and (25) into Eq.(28), the explicit form of the governing equations can be expressed with respect to the laminate stiffnesses E_{ij}. Eq.(28) is most general form for axial-flexural-torsional behavior of thin-walled composite beams, and the dependent variables W, U, V and Φ are fully coupled.

VI. FINITE ELEMENT FORMULATION

The present theory for thin-walled composite beams described in the previous section was implemented via a displacement based finite element method. The generalized displacements are expressed over each element as a combination of the one-dimensional linear Lagrange interpolation function Ψ_j and Hermite-cubic interpolation function ψ_j associated with node j and the nodal values

$$W = \sum_{j=1}^{2} w_j\Psi_j \tag{30a}$$

$$U = \sum_{j=1}^{4} u_j\psi_j \tag{30b}$$

$$V = \sum_{j=1}^{4} v_j\psi_j \tag{30c}$$

$$\Phi = \sum_{j=1}^{4} \phi_j\psi_j \tag{30d}$$

Substituting these expressions into the weak statement in Eq.(23), the finite element model of a typical element

can be expressed as

$$\big[K(\{\Delta\})\big]\{\Delta\} = \{f\} \tag{31}$$

The nonlinear algebraic equations of present theory can be linearized using Newton−Raphson iterative method. Solution of Eq.(31) by the Newton−Raphson iteration method results in the following linearized equations for the incremental solution at the r^{th} iteration (Bathe [24])

$$\big[T(\{\Delta\}^{r-1})\big]\{\delta\Delta\} = -\{R(\{\Delta\}^{r-1})\} \tag{32}$$

where the tangent stiffness matrix is calculated using the definition

$$\big[T(\{\Delta\}^{r-1})\big] \equiv \Big(\frac{\partial\{R\}}{\partial\{\Delta\}}\Big)^{r-1} \tag{33}$$

The residual vector vector after the $(r-1)^{th}$ iteration is given by

$$\{R(\{\Delta\}^{r-1})\} = [K(\{\Delta\}^{r-1})]\{\Delta\}^{r-1} - \{f\} \tag{34}$$

The solution at the r^{th} iteration is then given by

$$\{\Delta\}^{r} = \{\Delta\}^{r-1} + \{\delta\Delta\} \tag{35}$$

In Eq.(31), $\{\Delta\}$ is the unknown nodal displacements

$$\{\Delta\} = \{W\ U\ V\ \Phi\}^{\mathrm{T}} \tag{36}$$

VII. NUMERICAL EXAMPLES

Throughout numerical examples, a tolerance of $\epsilon = 10^{-3}$ and maximum allowable iterations of 20 (per load step) are used to check for convergence of nodal displacements in the Newton−Raphson iteration scheme. The initial solution vector is chosen to be the zero vector, so that the first iteration solution corresponds to the linear solution. Plane stress assumption ($\sigma_s = 0$) is used in the numerical computation. The results of the present analysis are given for both the linear and nonlinear case.

For verification purpose, a cantilever thin-walled composite Z-beam with geometry and three lay-ups under an eccentric transverse load of P=4.54N at free end is performed (Fig.2). All computations are carried out with the following material properties: $E_1 = 206.8$GPa $, E_2 = 103.4$GPa $, G_{12} = 51.7$GPa $, \nu_{12} = 0.30$. The tip rotations and deflections of present model are given in Table I, along with the analytical results of Gupta and Rao [12] and

Rajasekaran and Nalinaa [17] and FEAST-C [25]. The proposed model agrees well with previously available results and can capture exactly all the geometrical nonlinear response of composite beam. In order to investigate the influence of warping restraint effect on the nonlinear response, Harursampath [26] further analyzed this example by considering an eccentric transverse load of P=454N. By using two different boundary conditions at free end: restrained warping and free warping, the study is made with the symmetric $[0°/45°/0°]$ and anti-symmetric $[45°/-45°]$ lay-ups. Tables II and III show a good agreement between the results of the approach proposed herein and previous results. It should be noted that there is no difference results between free and restrained warping models, except for the axial and torsional displacements in Ref.[26]. For restrained warping model, it seems that the nonlinear results in Ref.[26] were calculated by assuming that the beam is restrained both warping and axially at the free end. Whereas, for free warping model, this beam is probably supposed free warping at both free ends. As expected, with two lay-ups considered, for linear analysis, the warping restraint has a stiffening effect. That is, the influence of the warping restraint becomes immaterial for all displacements, except for the angle of twist. However, it becomes significant and depends on types of lay-ups for nonlinear analysis. When comparing with free warping model, all the nonlinear displacements decrease for the symmetric lay-up, whereas they increase for anti-symmetric one.

Next, a cantilever symmetrically laminated symmetric I-beam with length $l = 2.5$m under a tip vertical load 250N at the free end is investigated. Following dimensions for I-beam are used: both of flanges width and web height are 50mm. The flanges and web are made of sixteen layers with each layer 0.13mm in thickness. All computations are carried out for the glass-epoxy materials with the following material properties: $E_1 = 53.78$GPa , $E_2 = 17.93$GPa , $G_{12} = 8.96$GPa , $\nu_{12} = 0.25$. For comparison, the axial and vertical displacements at the free end by this study and the results by 600 nine-noded ABAQUS's shell elements (S9R5) [27] are presented. The accuracy of the predictions from present model with the ABAQUS's solutions can be seen in Table IV for all lamination schemes considered.

In order to demonstrate the accuracy, generality and robustness of this study further, the buckling behavior of simply supported and cantilever composite mono-symmetric I-beam with length $l = 4.0$m under axial force at the centroid is performed. Lay-ups and material properties are the same with previous example except the geometry of I-section. The top and bottom flange widths are 30mm and 50mm, and web height are 50mm, respectively. The critical buckling loads obtained from present model are compared with those of Lee et al. [28] and Kim et al.[29], which are based on the linear bifurcation buckling theory and ABAQUS solution. The results of the different methods are found again to be in a good agreement in Table V. Load versus the lateral displacement of fiber angle $\theta = 30°$ and $60°$ in the flanges and web with different values of initial loading imperfections in x-direction ($V_x = 0.01$N, 0.05N and 0.10N) are

plotted in Figs. 3 and 4. The load versus lateral displacement curve monotonically increases and approaches a linear bifurcation buckling load value, which is characteristic of an incipient limit-point response of the beam. This response is also justified by the fact that the value of the limit-point load decreases with increasing imperfection amplitude.

A pinned-hinged composite I-beam of length $L = 8$m under an eccentric uniform load q acting at the left of the top flange is considered in order to investigate the effects of the load parameter and fiber orientation on the nonlinear flexural-torsional behavior. The geometry and stacking sequence of composite I-beam is shown in Fig.5, and the following engineering constants are used

$$E_1/E_2 = 25, G_{12}/E_2 = 0.6, \nu_{12} = 0.25 \tag{37}$$

For convenience, the following nondimensional values of the lateral, vertical displacement, and load parameter are used

$$\overline{u} = \frac{u}{b_3} \tag{38a}$$

$$\overline{v} = \frac{v}{b_3} \tag{38b}$$

$$\overline{q} = \frac{qL^4}{E_2 b_3^3 t_1} \tag{38c}$$

Stacking sequence of this beam consists of four layers with equal thickness as follows: $[\theta/-\theta]_2$ at the bottom flange and unidirectional at the web and top flange, respectively. For this lay-up, the coupling stiffnesses E_{15}, E_{16} and E_{35} do not vanish due to unsymmetric stacking sequence of the flanges. Accordingly, this beam sustains two kinds of couplings from material anisotropy and geometric nonlinearity simultaneously.

As the first example, the stacking sequence at two specific fiber angle $\theta = 30°, 90°$ is considered to study the effects of load parameter on the displacements in the high nonlinear region. It should be noted that for $\theta = 90°$, all the coupling stiffness vanish, that is, only geometrical nonlinear effect exists. The load with increment of $\Delta\overline{q} = 0.05$ is increased until the first critical point is reached. The solutions of the linear analysis are also presented to highlight the difference between linear and nonlinear responses with increasing load. Load versus the vertical displacement and load versus the angle of twist at two fiber angles are shown in Figs.6 and 7. It is evident that the linear theory is adequate in a relatively large region up to the point where the applied load reaches value of $\overline{q} = 0.5$ and 1 for fiber angle $\theta = 90°$ and $30°$, respectively. The results by nonlinear analysis are always larger than those of linear analysis. This is due to the fact that the geometrical nonlinear effect causes flexural-torsional coupling which results in a decrease in the flexural and torsional stiffness of the beam. The effect of the geometric nonlinearity is apparent with increasing load intensity. The highest load of fiber angle $\theta = 90°$ is smaller than that of $\theta = 30°$. At this load

of $\theta = 90°$, the nonlinear vertical and torsional displacements are about twice of those of linear analysis. It is from Fig.8 that highlights the influence of geometrical nonlinear effect on the lateral displacement of beam. This response is never seen in linear analysis because lateral displacement is decoupled with vertical and torsional load. It implies that the structure under an eccentric transverse load not only causes the transverse displacement and angle of twist as would be observed in linear case, but also causes an additional response due solely to geometric nonlinearity which does not occur in linear case.

To investigate the geometrical nonlinear effect further, the same configuration with the previous example except the load and laminate stacking sequence is considered. A pinned-hinged composite I-beam under a constant applied load is analyzed while the fiber angle is rotated in the bottom flange. Based on previous numerical example, an applied load $\overline{q} = 1.25$ is chosen to show effect of fiber orientation on the flexural-torsional response. Variation of the lateral, vertical and torsional displacements with respect to fiber angle change are illustrated in Figs.9 and 10. As expected, no linear lateral displacement $\bar{u}$ is seen for all fiber angles. For fiber angles less than $\theta = 30°$, the vertical displacement of linear and nonlinear analysis coincide. Especially, in Fig.10, the angle of twist of two analyzes shows the same tendency and reaches minimum value between fiber angle $\theta \in [10° - 20°]$, that is, because the torsional rigidity E_{55} becomes maximum value at this range. However, as the fiber orientation is rotated off-axis, geometrical nonlinear effect is prominent, that is, the discrepancy between the linear and nonlinear analysis becomes significant. The nonlinear vertical displacement is not as sensitive as the nonlinear lateral and torsional displacements when fiber angle changes. The difference between these displacements of two analyses is minimum at $\theta = 0°$ and reaches maximum value at $\theta = 90°$. This phenomenon can be explained that the axial, flexural and torsional rigidities decrease significantly with increasing fiber angle, and thus, the relative geometrical nonlinear effect becomes larger for higher fiber angles.

VIII. CONCLUDING REMARKS

A geometrically nonlinear model is developed to study the flexural-torsional behavior of general thin-walled open-section composite beams with arbitrary lay-ups under various types of loadings. This model is capable of predicting accurately nonlinear flexural-torsional response for various configuration including boundary conditions and laminate orientation of thin-walled composite beams. The nonlinear governing equations are derived from the principle of the stationary value of total potential energy and solved by means of an incremental Newton−Raphson method. A displacement-based one-dimensional finite element model that accounts for the geometric nonlinearity in the von Kármán sense is developed to solve the problem. The present model is found to be appropriate and efficient in

analyzing nonlinear flexural-torsional behavior of thin-walled composite beams.

Acknowledgments

The support of the research reported here by Korea Ministry of Construction and Transportation through Grant 2006-C106A1030001-06A050300220 and Seoul R&BD Program through Grant GR070033 is gratefully acknowledged. The authors also would like to thank the anonymous reviewers for their suggestions in improving the standard of the manuscript.

APPENDIX

The explicit forms of the laminate stiffnesses E_{ij} for composite I-section in Fig.11 can be defined by

$$\begin{aligned}
E_{16} &= (-2y_2+2y_p)B^1_{11}b_1 + D^1_{11}b_1 + (-2y_2+2y_p)B^2_{11}b_2 + D^2_{11}b_2 + (2x_3-2x_p)B^3_{11}b_3 + D^3_{11}b_3 \\
&+ (2y_1-2y_p)B^4_{11}b_4 + D^4_{11}b_4 + (2y_1-2y_p)B^5_{11}b_5 + D^5_{11}b_5 \qquad (39a)\\
E_{26} &= \frac{1}{2}((-2y_2+2y_p)B^1_{11} + D^1_{11})b_1^2 + (-2y_2+2y_p)(-b_1+x_3)B^1_{11}b_1 + D^1_{11}(-b_1+x_3)b_1 \\
&+ \frac{1}{2}((-2y_2+2y_p)B^2_{11} + D^2_{11})b_2^2 + (-2y_2+2y_p)x_3B^2_{11}b_2 + D^2_{11}x_3b_2 \\
&+ (2x_3-2x_p)x_3B^3_{11}b_3 + D^3_{11}(3x_3-2x_p)b_3 + F^3_{11}b_3 \\
&+ \frac{1}{2}((-2y_1+2y_p)B^4_{11} - D^4_{11})b_4^2 + (2y_1-2y_p)(b_4+x_3)B^4_{11}b_4 + D^4_{11}(b_4+x_3)b_4 \\
&+ \frac{1}{2}((-2y_1+2y_p)B^5_{11} - D^5_{11})b_5^2 + (2y_1-2y_p)x_3B^5_{11}b_5 + D^5_{11}x_3b_5 \qquad (39b)\\
E_{36} &= (-2y_2+2y_p)y_2B^1_{11}b_1 + D^1_{11}(3y_2-2y_p)b_1 - F^1_{11}b_1 \\
&+ (-2y_2+2y_p)y_2B^2_{11}b_2 + D^2_{11}(3y_2-2y_p)b_2 - F^2_{11}b_2 \\
&+ \frac{1}{2}((2x_3-2x_p)B^3_{11} + D^3_{11})b_3^2 + (2x_3-2x_p)y_2B^3_{11}b_3 + D^3_{11}y_2b_3 \\
&+ (2y_1-2y_p)y_1B^4_{11}b_4 + D^4_{11}(3y_1-2y_p)b_4 + F^4_{11}b_4 \\
&+ (2y_1-2y_p)y_1B^5_{11}b_5 + D^5_{11}(3y_1-2y_p)b_5 + F^5_{11}b_5 \qquad (39c)\\
E_{46} &= \frac{1}{2}((-2y_2+2y_p)(-y_2+y_p)B^1_{11} + D^1_{11}(y_2-y_p) - F^1_{11})b_1^2 - (-2y_2+2y_p)CB^1_{11}b_1 \\
&+ D^1_{11}(-C-(-2y_2+2y_p)(-b_1+x_3-x_p))b_1 - F^1_{11}(-b_1+x_3-x_p)b_1 \\
&+ \frac{1}{2}((-2y_2+2y_p)(-y_2+y_p)B^2_{11} + D^2_{11}(y_2-y_p) - F^2_{11})b_2^2 + (-2y_2+2y_p)((-y_2+y_p)b_1-C)B^2_{11}b_2 \\
&+ D^2_{11}((-y_2+y_p)b_1 - C - (-2y_2+2y_p)(x_3-x_p))b_2 - F^2_{11}(x_3-x_p)b_2
\end{aligned}$$

$$
\begin{aligned}
&+ \frac{1}{2}((2x_3-2x_p)(x_3-x_p)B^3_{11}+D^3_{11}(-x_3+x_p)-F^3_{11})b_3^2+(2x_3-2x_p)((-y_2+y_p)b_1-C)B^3_{11}b_3\\
&+ D^3_{11}((-y_2+y_p)b_1-C-(2x_3-2x_p)(y_2-y_p))b_3-F^3_{11}(y_2-y_p)b_3\\
&+ \frac{1}{2}((2y_1-2y_p)(y_1-y_p)B^4_{11}+D^4_{11}(-y_1+y_p)-F^4_{11})b_4^2\\
&+ (2y_1-2y_p)(-(y_1-y_p)b_4+(x_3-x_p)b_3+(-y_2+y_p)b_1-C)B^4_{11}b_4\\
&+ D^4_{11}(-(y_1-y_p)b_4-(2y_1-2y_p)(-b_4-x_3+x_p)+(x_3-x_p)b_3+(-y_2+y_p)b_1-C)b_4\\
&- F^4_{11}(-b_4-x_3+x_p)b_4+\frac{1}{2}((2y_1-2y_p)(y_1-y_p)B^5_{11}\\
&+ D^5_{11}(-y_1+y_p)-F^5_{11})b_5^2+(2y_1-2y_p)((x_3-x_p)b_3+(-y_2+y_p)b_1-C)B^5_{11}b_5\\
&+ D^5_{11}(-(2y_1-2y_p)(-x_3+x_p)+(x_3-x_p)b_3+(-y_2+y_p)b_1-C)b_5-F^5_{11}(-x_3+x_p)b_5 \qquad (39d)\\
E_{56} &= D^1_{16}(-2y_2+2y_p)b_1+F^1_{16}b_1+D^2_{16}(-2y_2+2y_p)b_2+F^2_{16}b_2\\
&+ D^3_{16}(2x_3-2x_p)b_3+F^3_{16}b_3+D^4_{16}(2y_1-2y_p)b_4+F^4_{16}b_4+D^5_{16}(2y_1-2y_p)b_5+F^5_{16}b_5 \qquad (39e)\\
E_{66} &= (-4y_2+4y_p)(-y_2+y_p)D^1_{11}b_1+(-4y_2+4y_p)F^1_{11}b_1+H^1_{11}b_1\\
&+ (-4y_2+4y_p)(-y_2+y_p)D^2_{11}b_2+(-4y_2+4y_p)F^2_{11}b_2+H^2_{11}b_2\\
&+ (4x_3-4x_p)(x_3-x_p)D^3_{11}b_3+(4x_3-4x_p)F^3_{11}b_3+H^3_{11}b_3\\
&+ (4y_1-4y_p)(y_1-y_p)D^4_{11}b_4+(4y_1-4y_p)F^4_{11}b_4+H^4_{11}b_4\\
&+ (4y_1-4y_p)(y_1-y_p)D^5_{11}b_5+(4y_1-4y_p)F^5_{11}b_5+H^5_{11}b_5 \qquad (39f)\\
C &= \Big[\frac{1}{2}(-y_2+y_p)t_1b_1^2+\frac{1}{2}(-y_2+y_p)t_1b_2^2+(-y_2+y_p)b_1t_1b_2+\frac{1}{2}(x_3-x_p)t_3b_3^2+(-y_2+y_p)b_1t_3b_3\\
&+ \frac{1}{2}(y_1-y_p)t_2b_4^2+(-(y_1-y_p)b_4+(x_3-x_p)b_3+(-y_2+y_p)b_1)t_2b_4+\frac{1}{2}(y_1-y_p)t_2b_5^2\\
&+ ((x_3-x_p)b_3+(-y_2+y_p)b_1)t_2b_5\Big]/(t_1b_1+t_1b_2+t_3b_3+t_2b_4+t_2b_5) \qquad (39g)
\end{aligned}
$$

Other values of E_{ij} can be found in Ref.[22].

References

[1] V. Z. Vlasov, Thin Walled Elastic Beams, Israel Program for Scientific Transactions, Jerusalem, 1961.

[2] A. Gjelsvik, The theory of thin walled bars, Wiley, New York, 1981.

[3] K. Bathe, S. Bolourchi, Large displacement analysis of three-dimensional beam structures, Int J Numer Meth Eng 14(7) (1) (1979) 961–986.

[4] D. H. Hodges, A. R. Atilgan, C. E. S. Cesnik, M. V. Fulton, On a simplified strain energy function for geometrically nonlinear behavior of anisotropic beams, in: European Rotorcraft Forum, 17th, Berlin, Germany, 1991.

[5] C. E. S. Cesnik, D. H. Hodges, A new concept for composite rotor blade cross-sectional modeling, J Am Helicopter Soc 42(1) (1997) 27–38.

[6] V. V. Volovoi, D. H. Hodges, C. E. S. Cesnik, B. Popescu, Assessment of beam modeling methods for rotor blade applications, Math Comput Model 33 (10-11) (2001) 1099–1112.

[7] W. Yu, V. Volovoi, D. Hodges, X. Hong, Validation of the variational asymptotic beam sectional analysis., AIAA J 40 (10) (2002) 2105–2112.

[8] W. Yu, D. H. Hodges, V. V. Volovoi, E. D. Fuchs, A generalized Vlasov theory for composite beams, Thin-Walled Struct 43 (9) (2005) 1493–1511.

[9] W. Yu, D. H. Hodges, Generalized Timoshenko Theory of the Variational Asymptotic Beam Sectional Analysis, J Am Helicopter Soc 50 (1) (2005) 46–55.

[10] N. Bauld, L. Tzeng, A Vlasov theory for fiber-reinforced beams with thin-walled open cross section, Int J Solids Struct 20 (3) (1984) 277–297.

[11] R. Gupta, K. Rao, Instability of laminated composite thin-walled open-section beams, Compos Struct 4(4) (1985) 299–313.

[12] R. Gupta, K. Rao, Finite element analysis of laminated anisotropic thin-walled open-section beams, Compos Struct 3(1) (1985) 19–31.

[13] K. Bhaskar, L. Librescu, A geometrically non-linear theory for laminated anisotropic thin-walled beams, Int J Eng Sci 33 (9) (1995) 1331 – 1344.

[14] L. Librescu, O. Song, Thin-Walled Composite Beams: Theory and Application (Solid Mechanics and Its Applications), 1st Edition, Springer, 2006.

[15] B. Omidvar, A. Ghorbanpoor, Nonlinear FE Solution for Thin-Walled Open-Section Composite Beams, J Struct Eng 122 (11) (1996) 1369–1378.

[16] F. Fraternali, L. Feo, On a moderate rotation theory of thin-walled composite beams, Compos Part B 31 (2) (2000) 141–158.

[17] S. Rajasekaran, K. Nalinaa, Stability and vibration analysis of non-prismatic thin-walled composite spatial members of generic section, Int J Struct Stabil Dynam 5 (4) (2005) 489–520.

[18] S. P. Machado, V. H. Cortinez, Non-linear model for stability of thin-walled composite beams with shear deformation, Thin-Walled Struct 43 (10) (2005) 1615 – 1645.

[19] V. H. Cortinez, M. T. Piovan, Stability of composite thin-walled beams with shear deformability, Comput Struct 84 (15-16) (2006) 978 – 990.

[20] S. P. Machado, Geometrically non-linear approximations on stability and free vibration of composite beams, Eng Struct 29 (12) (2007) 3567 – 3578.

[21] J. B. Cardoso, N. M. Benedito, A. J. Valido, Finite element analysis of thin-walled composite laminated beams with

geometrically nonlinear behavior including warping deformation, Thin-Walled Struct 47 (11) (2009) 1363–1372.

[22] J. Lee, S. Lee, Flexural-torsional behavior of thin-walled composite beams, Thin-Walled Struct 42 (9) (2004) 1293 – 1305.

[23] R. M. Jones, Mechanics of Composite Materials, Taylor & Francis, 1999.

[24] K. Bathe, Finite Element Procedures, 1996.

[25] Anonymous, Vikram Sarabai Space Center (VSSC), FEAST-C, User Manual (SEG, SDS Group, ISRO, Trivandrum, 1995).

[26] D. Harursampath, Non-classical non-linear effects in thin-walled composite beams, Ph.D. thesis, Georgia Institute of Technology, Atlanta, Georgia, U.S.A (1998).

[27] ABAQUS. Standard user's manual. ver 6.5-1. Hibbitt, Karlsson & Sorensen Inc; 2004.

[28] J. Lee, S. E. Kim, Flexural-torsional buckling of thin-walled I-section composites, Comput Struct 79 (10) (2001) 987 – 995.

[29] N. I. Kim, D. K. Shin, M. Y. Kim, Flexural-torsional buckling loads for spatially coupled stability analysis of thin-walled composite columns, Adv Eng Softw 39 (12) (2008) 949 – 961.

CAPTIONS OF TABLES

Table I: The tip rotations and deflections of a cantilever Z-beam under an eccentric transverse load P=4.45N.

Table II: The tip rotations and deflections of a cantilever $[0°/45°/0°]$ Z-beam under an eccentric transverse load P=445N.

Table III: The tip rotations and deflections of a cantilever $[45°/-45°]$ Z-beam under an eccentric transverse load P=445N.

Table IV: The tip axial and vertical displacements of a cantilever composite I-beam with symmetric angle-ply laminates $[\pm\theta]_{4s}$ in the flanges and web under a vertical load P= 250N at free end.

Table V: Critical bucking loads (N) of a simply supported and cantilever composite mono-symmetric I-beam with symmetric angle-ply laminates $[\pm\theta]_{4s}$ in the flanges and web.

CAPTIONS OF FIGURES

Figure 1: Definition of coordinates and generalized displacements in thin-walled open-sections.

Figure 2: A cantilever composite Z-beam under an eccentric transverse load and three stacking sequences.

Figure 3: Load versus the lateral displacement at mid-span of a simply supported composite mono-symmetric I-beam under different values of initial loading imperfections with the fiber angle 30° and 60° in the flanges and web.

Figure 4: Load versus the lateral displacement at free end of a cantilever composite mono-symmetric I-beam under different values of initial loading imperfections with the fiber angle 30° and 60° in the flanges and web.

Figure 5: A pinned-hinged composite I-beam under an eccentric uniform load.

Figure 6: Load versus the vertical displacement at mid-span of a pinned-hinged composite I-beam under an eccentric uniform load with the fiber angle 30° and 90° in the bottom flange.

Figure 7: Load versus the angle of twist at mid-span of a pinned-hinged composite I-beam under an eccentric uniform load with the fiber angle 30° and 90° in the bottom flange.

Figure 8: Load versus the lateral displacement at mid-span of a pinned-hinged composite I-beam under an eccentric uniform load with the fiber angle 30° and 90° in the bottom flange.

Figure 9: Variation of the vertical and lateral displacements at mid-span of a pinned-hinged composite I-beam under an eccentric uniform load with respect to fiber angle change in the bottom flange.

Figure 10: Variation of the angle of twist at mid-span of a pinned-hinged composite I-beam under an eccentric uniform load with respect to fiber angle change in the bottom flange.

Figure 11: Geometry of thin-walled composite I-beam.

TABLE I The tip rotations and deflections of a cantilever Z-beam under an eccentric transverse load P=4.45N.

Lay-ups	Formulation	W (mm)	U (mm)	V (mm)	V'(10^{-5} rad)	Φ(10^{-5} rad)
	Ref.[12]	0.0000	0.0215	0.0144	4.260	56.600
$[0°]$	Ref.[17]	0.0003	0.0230	0.0147	4.350	56.900
	Ref.[25]	0.0002	0.0216	0.0156	4.540	56.700
	Present	0.0000	0.0230	0.0154	4.547	57.653
	Ref.[12]	0.0000	0.0209	0.0312	6.190	56.400
$[45°/-45°]$	Ref.[17]	0.0005	0.0214	0.0303	6.320	54.800
	Ref.[25]	0.0004	0.0236	0.0341	8.120	58.200
	Present	0.0001	0.0235	0.0351	6.950	60.166
	Ref.[12]	0.0000	0.0161	0.0239	4.750	58.400
$[0°/45°/0°]$	Ref.[17]	0.0004	0.0164	0.0227	4.850	58.800
	Ref.[25]	0.0002	0.0177	0.0247	5.440	57.790
	Present	0.0000	0.0174	0.0260	5.136	59.833

TABLE II The tip rotations and deflections of a cantilever [0°/45°/0°] Z-beam under an eccentric transverse load P=445N.

Rotations/	Restrained Warping			Free Warping			
Deflections	Present		Ref.[26]	Present		Ref.[26]	
	Linear	Nonlinear	Linear-Nonlinear	Linear	Nonlinear	Linear	Nonlinear
W (mm)	0.0000	-0.0129	0.0000	0.0000	-0.0152	0.0000	0.0530
U (mm)	-2.5952	-2.6690	-2.6380	-2.5950	-2.7162	-2.6380	-2.6380
U'(10^{-3} rad)	-7.6626	-7.8039	-7.7910	-7.6606	-7.8403	-7.7910	-7.7910
V (mm)	1.7378	1.8141	1.7590	1.7377	1.8654	1.7590	1.7590
V'(10^{-3} rad)	5.1312	5.4078	5.1940	5.1305	5.6945	5.1940	5.1940
Φ(rad)	0.0308	0.0324	0.0309	0.0598	0.0631	0.2796	0.3166

TABLE III The tip rotations and deflections of a cantilever $[45^\circ/-45^\circ]$ Z-beam under an eccentric transverse load P=445N.

Rotations/	Restrained Warping			Free Warping			
Deflections	Present		Ref.[26]	Present		Ref.[26]	
	Linear	Nonlinear	Linear-Nonlinear	Linear	Nonlinear	Linear	Nonlinear
W (mm)	0.0078	-0.0127	0.0000	0.0133	-0.0069	0.0922	-0.0178
U (mm)	-3.5173	-3.3467	-3.5580	-3.5173	-3.1442	-3.5580	-3.5580
U'(10^{-3} rad)	-10.3860	-9.7883	-10.5100	-10.3860	-8.9969	-10.5100	-10.5100
V (mm)	2.3540	2.3392	2.3720	2.3540	2.2718	2.3720	2.3720
V'(10^{-3} rad)	6.9508	6.9795	7.0030	6.9508	6.8550	7.0030	7.0030
Φ(rad)	0.0352	0.0348	0.0349	0.0602	0.0580	0.4183	0.4861

TABLE IV The tip axial and vertical displacements of a cantilever composite I-beam with symmetric angle-ply laminates $[\pm\theta]_{4s}$ in the flanges and web under a vertical load P= 250N at free end.

Lay-ups	Formulation	W (cm)	V (cm)
$[0]_{16}$	ABAQUS	-0.6124	15.9760
	Present	-0.6075	15.9113
$[15/-15]_{4s}$	ABAQUS	-0.7474	17.6434
	Present	-0.7432	17.6002
$[30/-30]_{4s}$	ABAQUS	-1.3416	23.6133
	Present	-1.3404	23.6384
$[45/-45]_{4s}$	ABAQUS	-2.7501	33.7463
	Present	-2.7600	33.9294
$[60/-60]_{4s}$	ABAQUS	-4.3164	42.2037
	Present	-4.3443	42.5798
$[75/-75]_{4s}$	ABAQUS	-5.0482	45.6077
	Present	-5.0838	46.0678
$[90/-90]_{4s}$	ABAQUS	-5.1983	46.2755
	Present	-5.2341	46.7453
$[0/90]_{4s}$	ABAQUS	-1.3488	23.6829
	Present	-1.3569	23.7830

TABLE V Critical bucking loads (N) of a simply supported and cantilever composite mono-symmetric I-beam with symmetric angle-ply laminates $[\pm\theta]_{4s}$ in the flanges and web.

Lay-ups	Simply supported beam				Cantilever beam	
	Lee et al. [28]	Kim et al. [29]		Present	Lee et al. [28]	Present
		ABAQUS	Theory			
$[0]_{16}$	842.28	837.40	842.30	841.00	216.76	216.50
$[15/-15]_{4s}$	768.03	766.80	768.30	767.00	196.25	196.00
$[30/-30]_{4s}$	577.11	577.30	577.80	576.00	146.15	146.00
$[45/-45]_{4s}$	401.65	402.40	402.50	401.00	101.31	101.25
$[60/-60]_{4s}$	318.08	318.80	318.80	318.00	80.18	80.00
$[75/-75]_{4s}$	292.77	293.10	293.10	292.00	73.85	73.75
$[90/-90]_{4s}$	288.15			288.00	72.72	72.50
$[0/90]_{4s}$	568.95	571.10	571.90	568.00	144.99	144.75

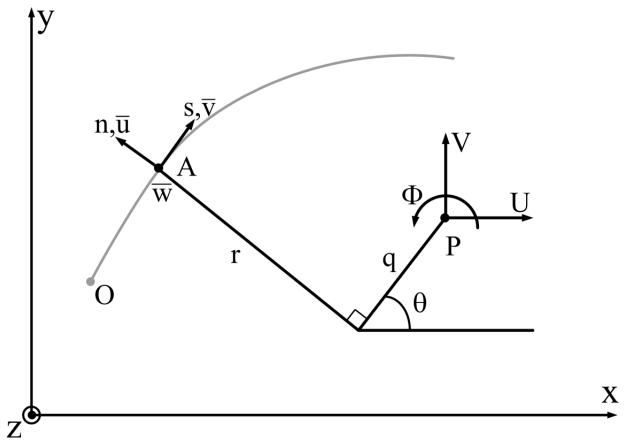

FIG. 1 Definition of coordinates and generalized displacements in thin-walled open-sections.

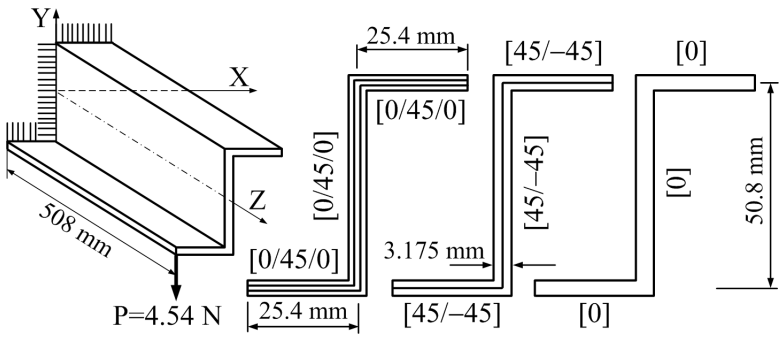

FIG. 2 A cantilever composite Z-beam under an eccentric transverse load and three stacking sequences.

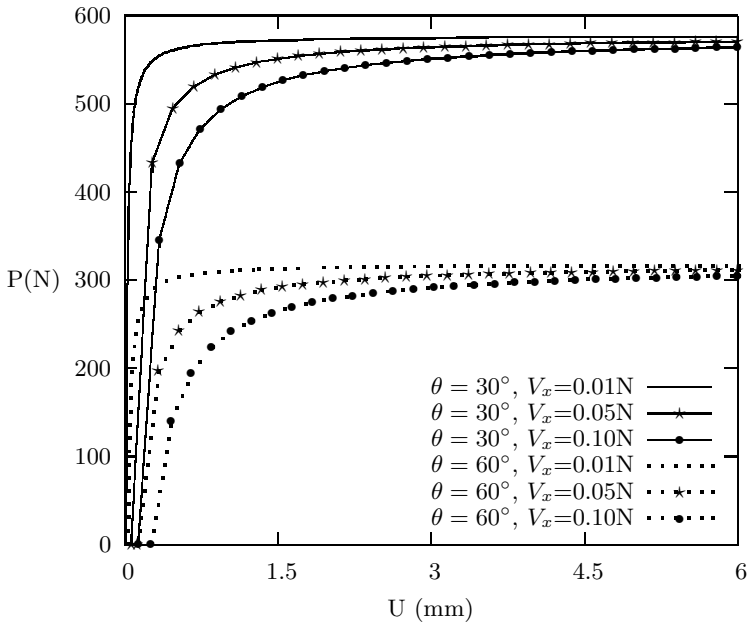

FIG. 3 Load versus the lateral displacement at mid-span of a simply supported composite mono-symmetric I-beam under different values of initial loading imperfections with the fiber angle 30° and 60° in the flanges and web.

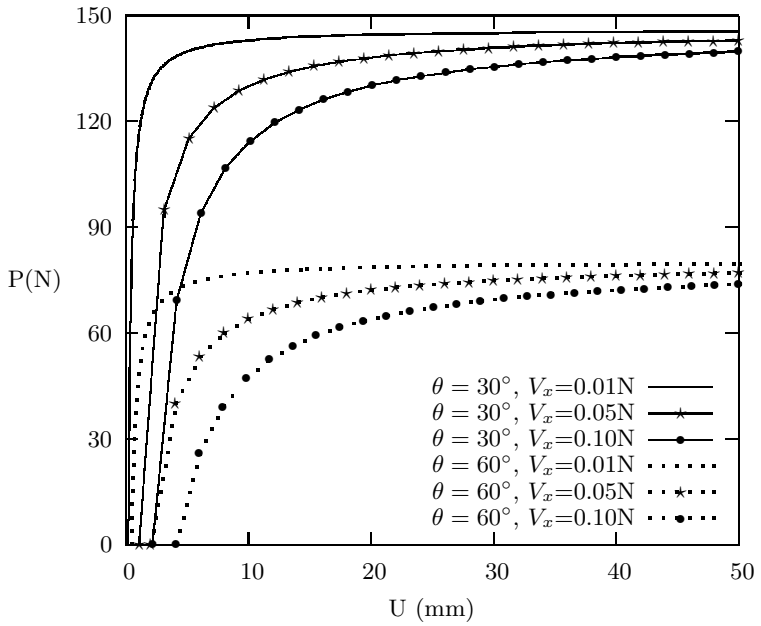

FIG. 4 Load versus the lateral displacement at free end of a cantilever composite mono-symmetric I-beam under different values of initial loading imperfections with the fiber angle 30° and 60° in the flanges and web.

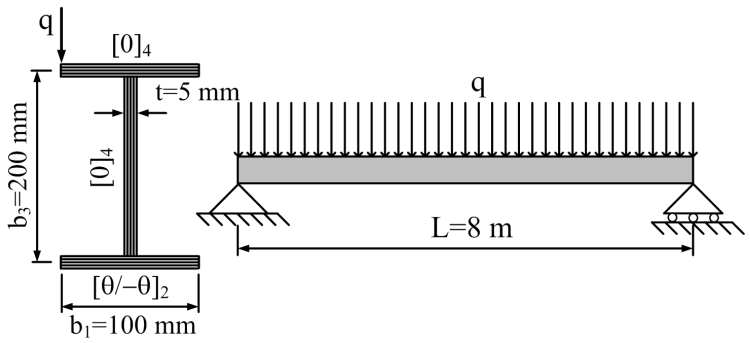

FIG. 5 A pinned-hinged composite I-beam under an eccentric uniform load.

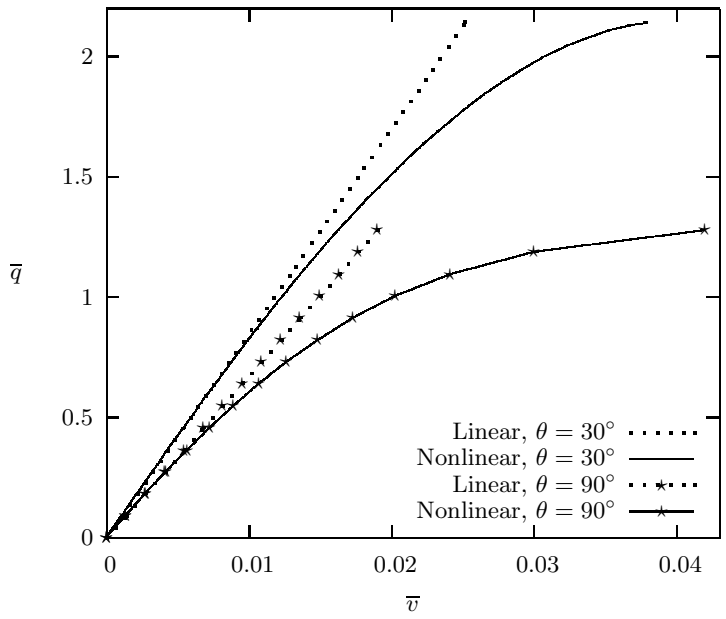

FIG. 6 Load versus the vertical displacement at mid-span of a pinned-hinged composite I-beam under an eccentric uniform load with the fiber angle 30° and 90° in the bottom flange.

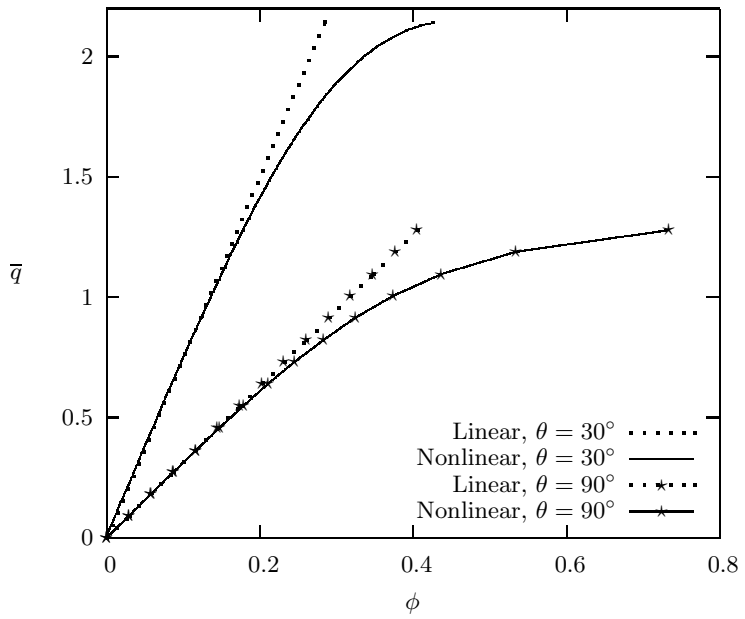

FIG. 7 Load versus the angle of twist at mid-span of a pinned-hinged composite I-beam under an eccentric uniform load with the fiber angle 30° and 90° in the bottom flange.

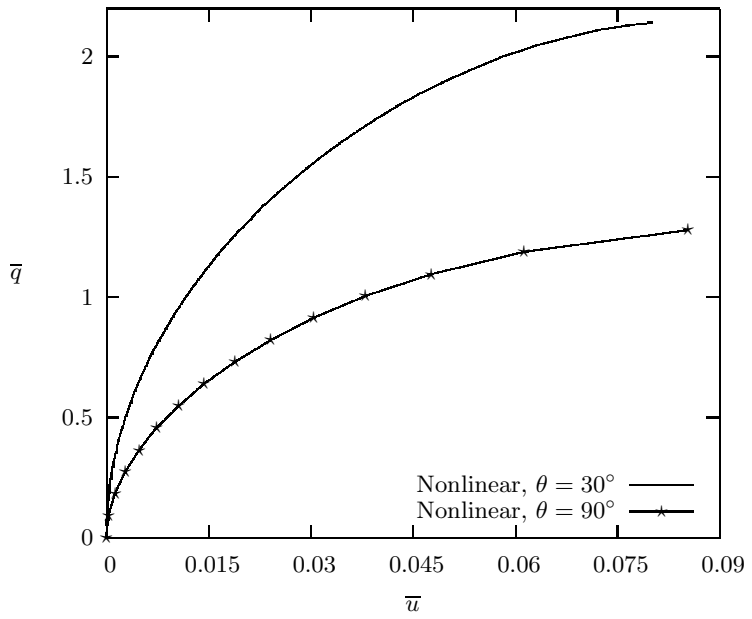

FIG. 8 Load versus the lateral displacement at mid-span of a pinned-hinged composite I-beam under an eccentric uniform load with the fiber angle 30° and 90° in the bottom flange.

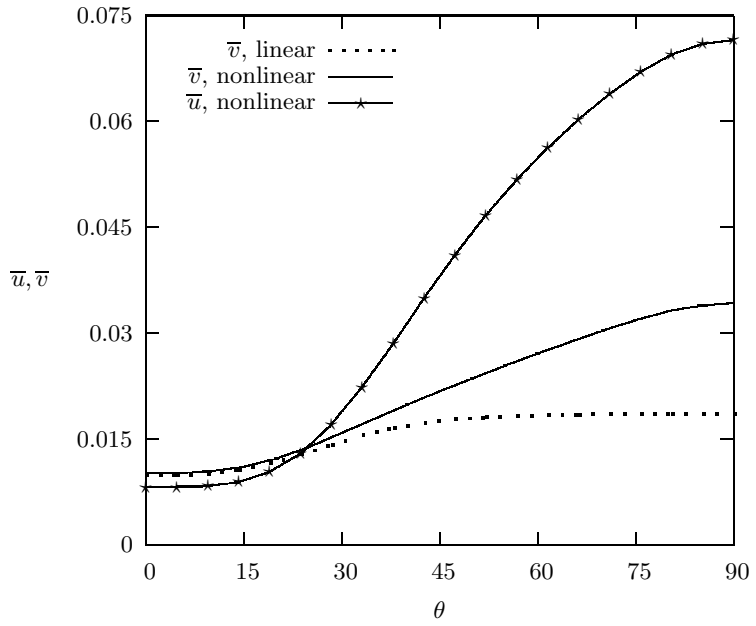

FIG. 9 Variation of the vertical and lateral displacements at mid-span of a pinned-hinged composite I-beam under an eccentric uniform load with respect to fiber angle change in the bottom flange.

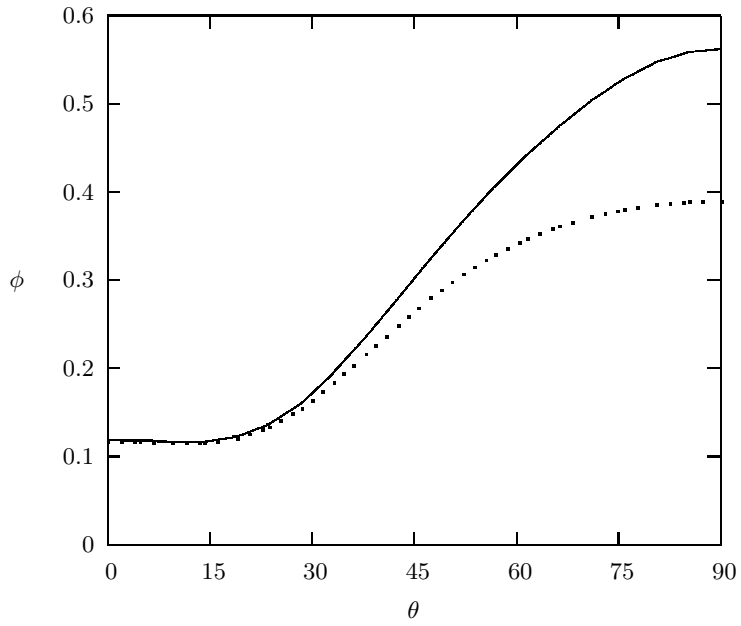

FIG. 10 Variation of the angle of twist at mid-span of a pinned-hinged composite I-beam under an eccentric uniform load with respect to fiber angle change in the bottom flange.

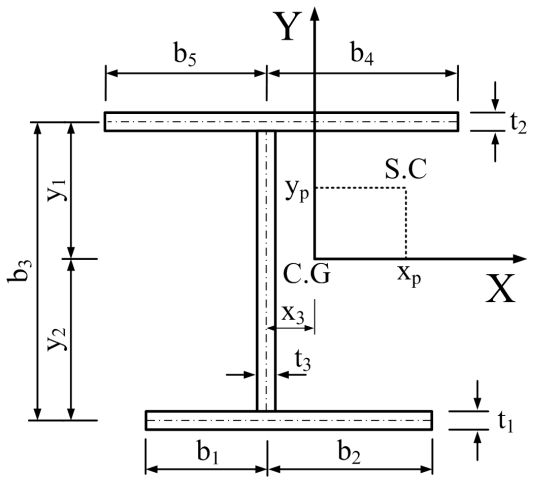

FIG. 11 Geometry of thin-walled composite I-beam.